IOP Conf. Series: Materials Science and Engineering **181** (2017) 012012 doi:10.1088/1757-899X/181/1/012012

Manufacture of iron-based, amorphous coatings with high fracture toughness

K Bobzin, M Öte and T Königstein

Surface Engineering Institute of RWTH Aachen University, Kackertstr. 15, 52072 Aachen, Germany

Abstract. Amorphous iron-based material have excellent corrosion behaviour, show good tribological performances and exhibit interesting thermophysical properties. The deposition as a coating system by thermal spraying technology is an innovative approach to manufacture these materials. In this study, the mechanical properties of three iron-based amorphous coatings with different chromium content x_{Cr} = 0, 5 and 15 at.% are presented deposited by means of High Velocity Oxygen Fuel Spraying. For the determination of the amorphous content the linear relationship between crystallization energy and amount of amorphous structures is used. Comparing the crystallization energies of amorphous ribbons manufactured by melt spinning to those of feedstock materials and free standing coatings, assumptions regarding the amorphous contents are drawn. The results show that the amorphous content in the feedstock material is influenced by the amount of chromium content. Furthermore, the amorphous content of all coatings do not exceed those of the feedstock materials. Powder x_{Cr} = 15 at.% and the corresponding coating exhibit smallest amount of amorphous structure, presumably due to a not fully melted state of the impacting particles. The values of fracture toughness of the coatings are determined by means of indentation and subsequent measurement of the crack lengths. Furthermore, values of indentation modulus and hardness are measured and compared to each other. While length of indentation cracks decreases with increasing chromium content, an increase in indention modulus and hardness is observed. In comparison to ceramic reference YSZ and the steel reference 1.4404, all amorphous coatings show promising properties such as low indentation crack lengths and high hardness.

1. Introduction

In order to produce amorphous materials, extremely high cooling rates in the order of $\dot{T} = 10^6$-10^7 K/s during the solidification are necessary. High cooling rates suppress the formation of crystalline structures and enable the formation of amorphous metastable phases. By means of thermal spraying, the above mentioned cooling rates can be reached and coatings with fully or partially amorphous microstructures can be manufactured. The chemical composition of the alloy is another factor which is decisive for the formation of amorphous structures. Alloys with a chemical composition consisting of FeBSiNb have been reported to be especially suitable for the formation of amorphous phases [1]. Due to the lack of crystalline structures, amorphous materials offer a good protection against selective corrosion, especially due to the absence of grain boundaries in the microstructure [2, 3, 4, 5]. Furthermore, amorphous materials exhibit high hardness and are therefore frequently discussed regarding their deployment in tribologically loaded components [4]. A major disadvantage of amorphous materials, on the other hand, is their low fracture toughness. Use of materials with high fracture toughness might be necessary for numerous applications, i.e. for systems which operate under

cyclic thermomechanical loading. Apart from corrosion resistance and tribological behavior of the applied coatings, thermophysical properties, i.e. thermal conductivity, have been examined in this study. The measured thermal conductivities amount, in some instances, are lower than $\kappa = 3{,}0$ W/(mK) [6, 7]. In comparison, the thermal conductivities of plasma sprayed Yttria stabilized Zirconia (YSZ) can be lower than $\kappa = 1{,}0$ W/mK [8]. Therefore, it can be stated that metallic glasses might also come into use in order to protect thermally loaded components, depending on the maximum temperatures, which the components are exposed to. The operating temperatures should be well below the melting temperature of the coatings and even less than their crystallization temperature, so that no crystallization occurs, which would change the thermal conductivity of the coating.

Within the scope of this study, FeCrBSiN coatings with varying Cr and Fe contents have been developed by altering the chemical composition of amorphous material presented in [1]. In this regard, the chromium content (x_{Cr}) of the coatings has been increased stepwise between x_{Cr} = 5 at. % and 15 at.%, while iron content has been decreased correspondingly. The aim was, to improve the oxidation resistance of the coatings by increasing the Cr content. The proportions of the amorphous phase in the developed coatings have been assumed by comparing the crystallization energy of examined specimens with that of a ribbon manufactured by means of melt spinning. The procedure, as introduced in [2, 5], will be explained in chapter 2 more in detail. Furthermore, the fracture toughness of the coatings has been analyzed. In order to evaluate the fracture toughness (K_{Ic}) of materials, a wide number of different approaches exist in the literature [9]. In this study the model according to Anstis et al. has been employed, see equation (1) [10]. In order to calculate the K_{Ic} factor the values for hardness (H), elastic modulus (E), indentation force (F) and crack length need to be determined. The experiments used in order to determine these values will be introduced in chapter 2. Subsequently the results will be discussed and conclusions will be given.

$$K_{Ic} = 0.016 \cdot \left(\frac{H}{E}\right)^{0.5} \cdot \frac{F}{c^{1.5}} \tag{1}$$

2. Test Methods

Three different $Fe_{72-x}Cr_xB_{20}Si_4Nb_4$ (x_{Cr} = 0, 5, 15) feedstock materials featuring different chromium contents were produced by means of gas atomization. The powders were sieved with a targeted powder fraction of -45 to +10 µm. It was confirmed by the measurements conducted using a specialized optical particle analyze system; Morphologi G2 by Malvern Instruments Ltd (Worcestershire, England), that the resulted powder fraction corresponds to the targeted one. Furthermore, single powder particles made of different feedstock materials were analyzed metallographically in cross-sections using scanning electron microscope (SEM) LEO 1530 VP Gemini by the company Carl Zeiss AG (Oberkochen, Germany). Subsequently, the inner crystalline structures of the powder particles were analyzed by means of X-Ray Diffractometry (XRD) using Seifert XRD 3003 from GE Sensing & Inspection Technologies GmbH (Hürth, Germany). For the XRD measurements a CuKα target was selected. The angle of incidence $\omega = 10°$, step with $2\Theta = 0.05°$, holding time t_h = 10 s and measurement interval between $2\Theta = 20°$ to 80° remained constant for all measurements. Moreover, all powders were analyzed by means of dynamic Differential Scanning Calorimetry (DSC) using SETSYS Evolution System of SETARAM Instrumentation (Caluire, France) in order to obtain melting temperatures. For the DSC measurements a sample weight of m_s = 20 mg and heating rates of $\dot{T}$ = 10 K/min were selected. Afterwards, the crystallization energies of the powders were determined by calculating the baseline integral value. A description of how to determine the energy values from DSC curves can be found in [11, 12]. In order to assess the proportions of amorphous structures within the feedstock material, said value is compared to the crystallization energy of a reference material manufactured by melt spinning process using the Melt Spinner SC by Edmund Bühler GmbH (Hechingen, Germany). Same approach can be found in [1]. The melt spinning process is designed such way that extremely high cooling rates can be realized. During the melt

spinning process the material is liquidized by means of induction. Subsequently, by increasing argon pressure the liquid material is pressed through a ceramic nozzle onto a rotating copper roller. Due to high thermal conductivity of copper high cooling rates can be realized allowing the manufacture of amorphous ribbons. For the manufacture of the reference specimens a slit-nozzle with the geometry of width w = 5 mm and broadness b = 0.7 mm was utilized. The distance between the nozzle and copper roller was s = 0.4 mm. The rotating frequency of the copper roller was set to f = 25 Hz. Within this study, it must be noted that this evaluation method regarding the amorphous content is based on the assumptions that the reference specimen exhibits a fully amorphous state and that the crystallization energy and amount of amorphous structure have a linear relationship. The calculation of the amorphous content of the powder is done by following equation (2). In this formula $x_{am,P}$ represents the amorphous content of the powder, Δh_P the crystallization energy of the powder and Δh_R the crystallization energy of the ribbon.

$$x_{am.P} = \frac{\Delta h_P}{\Delta h_R} \tag{2}$$

All amorphous iron-based feedstock materials were sprayed by High Velocity Oxygen Fuel spraying (HVOF) using K2 system of the company GTV Verschleißschutz GmbH (Luckenbach, Germany). Spraying distance s = 300 mm, Oxygen flow rate $\dot{V}_O$ = 800 SLPM and the traverse speed of the robot v_R = 1,000 mm/s were kept constant throughout the experiments. The nozzle has a length of l = 145 mm and a diameter of d = 12 mm. Flat discs made from AlSi10 were used as substrate. Prior to the coating process, the substrate's surface was roughened by means of grit blasting with corundum F24 exhibiting particle size of x_p = 600 - 850 µm. By means of an SEM, the coatings were examined with regard to their microstructures in metallographic cross-sections. All coatings were analyzed with regard to their crystalline composition via XRD. Free standing coatings were manufactured for DSC measurements and to determine the crystallization energy (Δh_C). The amorphous content of the coatings are calculated, by comparing the crystallization energy of the coatings to the ribbons.

For the determination of fracture toughness, crack network was initiated via indentation in a cross-section using a Vickers geometry. The tests were conducted according to DIN EN ISO 6507-1. For the generation of the networks of cracks, a test load of m = 3 kg (F = 29.43 N) was chosen. After the maximum load is reached, the load was kept constant for t = 10 s. Subsequently, the lengths of the horizontally running cracks were measured under a light microscope. Moreover, the indentation modulus and the universal hardness of the coatings were determined via Fischerscope of the type HM2000 by the company Fischer (Sindelfingen-Maichingen, Germany). All measurements were conducted with n = 10 repetitions for each material, thus ensuring statistical accuracy. For the purpose of comparison, an established ceramic thermal barrier coating system was used. It consists of a MCrAIY bond coat and a top layer made of YSZ. Apart from the ceramic material, a stainless steel coating made from 1.4404 was chosen for comparison as well.

3. Research Results

The SEM powder characterization has shown that all particles exhibit a spherical shape. The powder particles consisting of x_{Cr} = 15 at. % show a clear microstructure indicating the presence of crystalline structures. The presence of crystalline structure in this case has also been verified via XRD showing a high intensity peak at $2\Theta = 45°$, see figure 1a. This indicates a ferritic structure. Measurements via DSC have shown that the melting temperature of the feedstock material increases with increasing chromium content. The differences between the powder containing no chromium and that containing x_{Cr} = 15 at. % chromium, amounts to about ΔT = 70 °C. The calculated amorphous contents using equation (1) for different powders are presented in figure 1b. These results underline the XRD pattern, showing smallest amorphous content for powder x_{Cr} = 15 at. %. Feedstock material x_{Cr} = 5 % exhibits calculated values of almost x_{am} = 120 % indicating very high amount of amorphous structures. Here it

must be noted that values above x_{am} = 100 % does not have a physical meaning but shows that the powder exhibits a higher amorphous content than that of the manufactured ribbons. This can be attributed to high cooling rates during powder manufacturing process by gas atomization process.

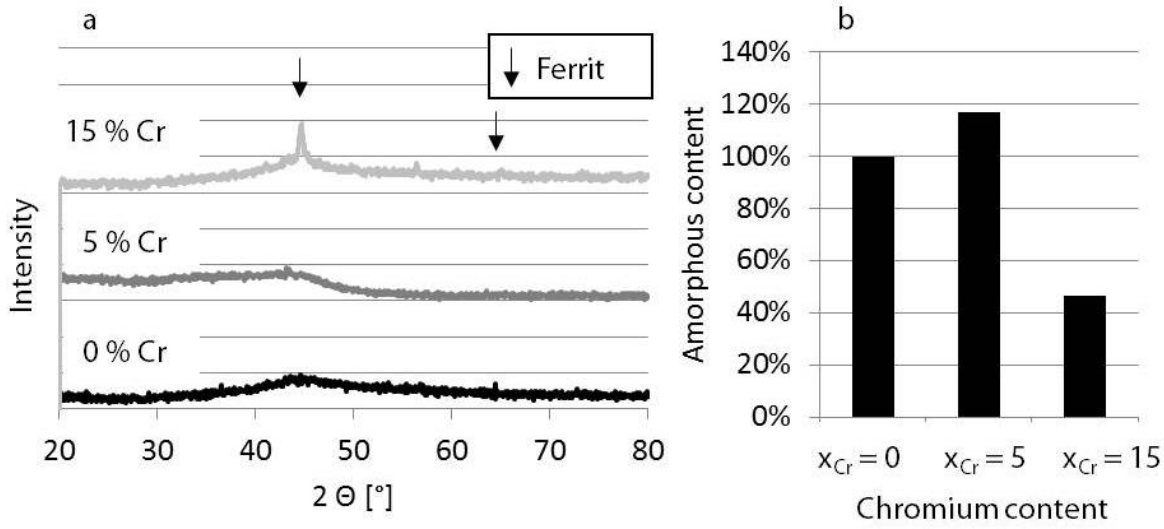

Figure 1. (a) XRD measurements and (b) calculated amorphous content of feedstock materials with different chromium contents.

In figure 2, cross-sectional views of different coatings applied in the context of this study have been presented. All coatings exhibit a dense microstructure as shown in figure 2. It can be observed that with increasing chromium content, the appearance of the voids and pores in the coating microstructure changes. Moreover, it must be noted that the coating thickness is significantly lower in case of the coating with highest chromium content, although all the process settings were the same in all experiments. Furthermore, for x_{Cr} = 15 at. % a high amount of spherical particles can be observed within the coating microstructure. It is likely, that the high melting temperature of this feedstock material, which is determined by means of DSC measurements to be almost ΔT = 70 °C higher than that of the other feedstock materials, restrict the melting behavior of some powder particles during their flight. Some of the arriving particles, which do not exhibit convenient melting degree, are not incorporated into the coating build-up and bounce back from the coating surface. These are exhausted from the coating chamber as overspray. Therefore, the reduction in the coating thickness in case of the feedstock material with a chromium content of x_{Cr} = 15 at. % can be attributed to the loss of some unmolten particles in overspray. Moreover, compression of the underlying splats due to the impact of arriving high-velocity unmolten particles might also be contributing to the reduction in coating thickness. Furthermore, the size, orientation and positions of the pores in the coating with x_{Cr} = 15 at. % differs compared to those with x_{Cr} = 0 at. % and 5 at. %. For the coating with x_{Cr} = 15 at. %, the majority of the pores range in size of a few micrometers. These cannot only be found between the splats, but also inside the unmolten particles. The low deformability of the feedstock materials together with the high impact velocity of the particles might be responsible for the formation of crack like structures within the deposited unmolten particles. These have in general a perpendicular orientation to the substrat's surface.

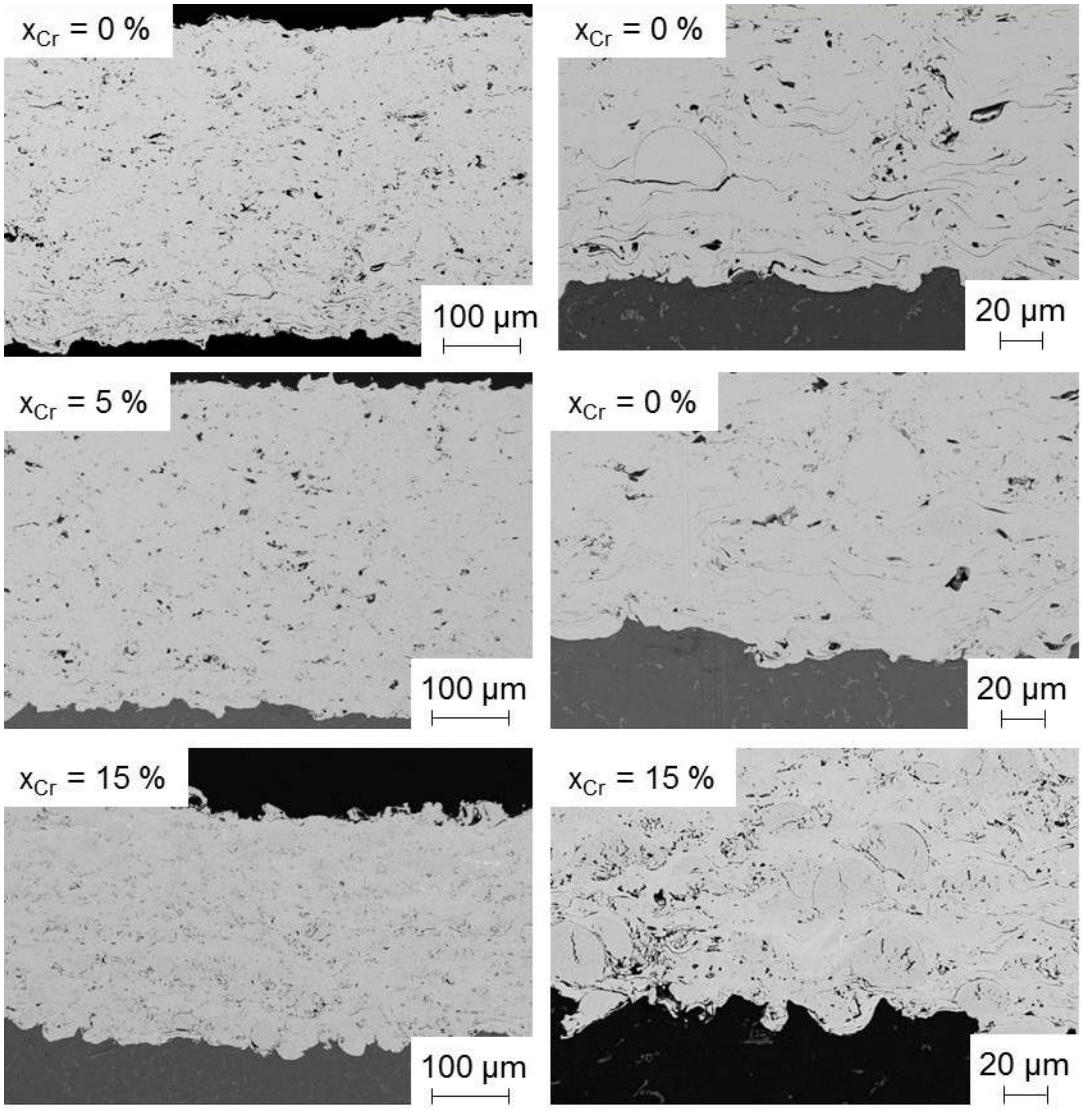

Figure 2. Cross-sections of coatings captured by means of SEM: left magnification 400x, right magnification 1,000x.

XRD measurements conducted on the deposited coatings do not reveal any phase transitions, as shown in figure 3. Coating deposited with x_{Cr} = 15 at. % remains crystalline or at least partly crystalline. Coatings deposited with x_{Cr} = 0 and 5 at. %, show a largely amorphous/nanocrystalline structure. This can be concluded from the characteristic halo pattern and a sharper peak at $2\Theta = 45°$ compared to the feedstock material. Additionally, DSC measurements were executed for quantification of the amorphous content. Comparing the results between the feedstock materials and coatings it can be observed, that the amorphous content of all coatings is significantly lower and amounts less than 50 % of the feedstock material. It is assumed that during coating process crystallization of the feedstock material occurs and nanocrystalline structures are formed. For the coating with x_{Cr} = 15 at. %, lowest amorphous content was observed, which is line with the XRD measurements.

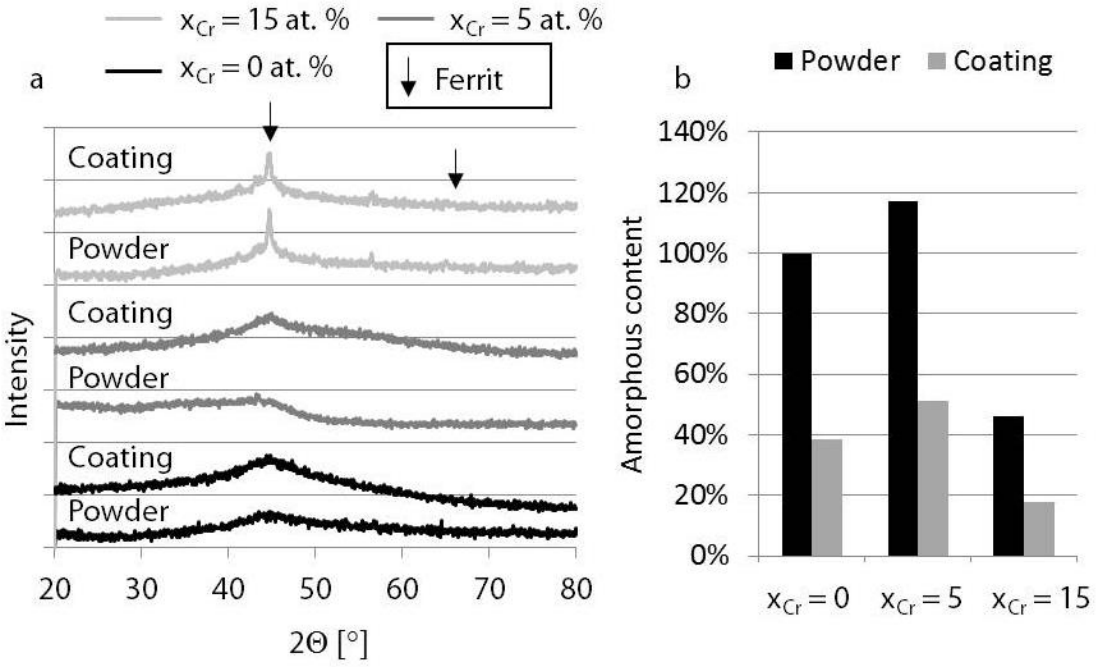

Figure 3. (a) XRD measurements and (b) calculated amorphous content of free standing coatings in comparison to feedstock materials with different chromium contents.

All coatings indicate the presence of partially amorphous structures. In the following for the sake of simplification these will be referred as amorphous coatings although these are not fully amorphous. For comparing the fracture toughness of the amorphous coatings, two references, a plasma sprayed YSZ coating and a plasma sprayed stainless steel 1.4404 coating, were manufactured. For both feedstock materials APS is the most frequently used spraying technology. From polished cross-section in figure 4 it can be seen that the coating made of 1.4404 exhibits areas of dark contrast. These areas most likely correspond to oxide inclusions. Part of these oxides are formed on the particle surface during particle flight in free jet. After impact with the substrate these oxides are incorporated into the coating, forming brittle phases. In comparison, the YSZ coating exhibits a porous microstructure. Neither lamellar coating build-up can be identified nor different phases can be distinguished by observing the cross-section. For the iron-based amorphous coating no oxide inclusions can be observed. The metallographic cross-section show highly deformed splats and a lamellar coating build up which is characteristic for metallic coatings deposited by HVOF.

By indentation into the polished cross-sections crack networks were initiated. Figure 4 shows both reference materials and exemplarily the coating with x_{Cr} = 5 at.% prior and subsequent to the indentation. Since for the reference material 1.4404, the determination of the crack length is difficult to follow in the illustration, it is marked with bars. As the oxides arrangement is largely interlamellarly, crack formation occurs at these brittle phases. For the iron-based amorphous coatings material separation occurs between single splats. As expected, largest cracks were observed in the coating made of YSZ.

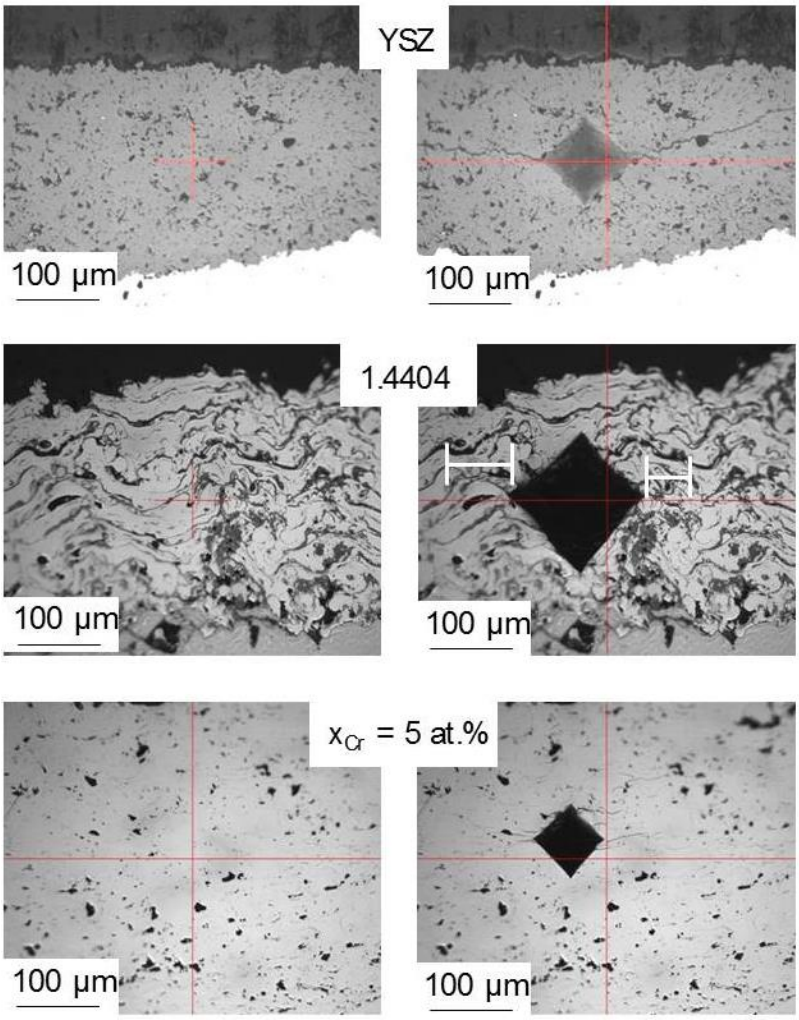

Figure 4. Examples of cross-sections prior and subsequent to indentation test.

For the calculation of the fracture toughness according to Anstis et al., among other values indentation modulus and hardness are required, which were determined by indentation into polished cross sections. In table 1 all results are summarized including standard deviations. It can be observed that for the amorphous iron-based coatings, indentation modulus and hardness increase with rising chromium content while the crack length decreases. The references 1.4404 and YSZ exhibit lower indentation modulus and hardness compared to amorphous coatings, while crack length is smallest for 1.4404 and largest for YSZ. Due to the fact that 1.4404 is rather ductile and YSZ rather brittle, these results were expected. For the determination of fracture toughness according to equation (1), the average values were used. Comparing the results from different iron-based amorphous coatings, it can be stated that the fracture toughness increases significantly with increasing chromium content in the coating. Due to the fact that the first term in equation (1), the ratio of hardness to the indentation modulus, does not show any significant changes between the examined samples, crack length must be the dominating factor affecting fracture toughnesses of the iron-based amorphous coatings. As expected YSZ coating exhibits the smallest fracture toughness with a value of K_{Ic} = 0.5 MPa·$m^{0.5}$. Similar results with regard to fracture toughness of YSZ coatings ranging between K_{Ic} = 1-2 MPa·$m^{0,5}$ were reported in the literature [13]. Comparing the fracture toughness of the iron-based amorphous coatings to the YSZ coating it can be seen that the iron-based coating exhibits 2 to 10 times higher fracture toughness values.

Table 1. Average values and standard deviations of indentation modulus (E), hardness (H), crack length (c) and average values of fracture toughness (K_{Ic}).

	E (GPa)	H (GPa)	c (µm)	$(E/H)^{0.5}$	K_{Ic} ($MPa \cdot m^{0.5}$)
x_{Cr} = 0 at.%	173.0 ± 6.4	9.2 ± 0.9	111.5 ± 42.3	4.3	1.7
x_{Cr} = 5 at.%	178.7 ± 9.5	10.1 ± 1.2	84.3 ± 27.2	4.2	2.6
x_{Cr} = 15 at.%	191.8 ± 13.2	10.2 ± 1.4	56.4 ± 14.0	4.3	4.9
YSZ	129.9 ± 13.3	8.4 ± 1.1	238.5 ± 68.4	3.9	0.5
1.4404	110.7 ± 11.0	3.1 ± 0.7	34.8 ± 22.4	5.9	14.1

4. Summary and outlook

Amorphous iron based materials are highly innovative materials and can be applied by means of Thermal Spray technology in form of coatings. The application areas have yet to be explored further, especially with regard to their deployment in tribological systems. Within this study, coatings manufactured by HVOF technology exhibit a partially amorphous structure. Comparing the amorphous content of the feedstock material and that of deposited coatings, a reduction in amorphous content is observed which can be explained by crystallization process during coating deposition. Nevertheless, a high amount of amorphous phase in the case of coating with a chromium content of x_{Cr} = 5 % could be realized. All amorphous coatings show high fracture toughnesses compared to a reference YSZ coating. These findings underline the potential of amorphous coatings with regard to application in tribological systems which will be part of future research.

Further studies will focus on how different thermal spray technologies influence the formation of amorphous structures. Special attention will be paid on air plasma spraying. Due to the higher processing temperatures, it is assumed that particles made of the feedstock material with x_{Cr} = 15 at. % will be molten entirely, thus enabling the formation of highly amorphous structures as well. Furthermore, the possibility to manufacture a wire with the same chemical composition will be discussed, which could then be used in Plasma Transferred Wire Arc (PTWA) technology for the deposition of coatings on inner geometries.

Acknowledgement

The authors gratefully acknowledge the financial support of the German Research Foundation (DFG) within the Project ‘Basic research on the applicability of Fe-based TS-coating with the purpose of thermal insulation’ (BO 1979/34-1).

References

[1] Amiya K, Urata A, Nishiyama N and Inoue A 2004 *Materials Transactions* **45(4)** 1214–18
[2] Zhou Z, Wang L, Wang F C, Zhang H F, Liu Y B and Xu S H 2009 *Surface & Coating Technology* **204** 563–70
[3] Liu G, An Y, Guo Z, Chen J, Hou G and Chen J 2012 *Applied Surface Science* **258** 5380–86
[4] Liu X Q, Zheng Y G, Chang X C, Hou W L, Qang J Q, Tang Z and Burgess A 2009 *Alloy and Compounds* **484** 300–7
[6] Shin D I, Gitzhofer F and Moreau C 2005 *Journal of Thermal Spray Technology* **16** 118–27
[5] Liu G, An Y, Guo Z, Chen J, Hou G and Chen J 2012 *Applied Surface Science* **258** 5380–86
[7] Shin D I, Gitzhofer F and Moreau C 2007 *Journal of Material Science* **42** 5915–23
[9] Sergejev F and Antonov M 2006 Comparative study on indentation fracture toughness measurements of cemented carbides *Proc. Estonian Acad. Sci. Eng.* **12(4)** 388–98
[8] Dutton R, Wheeler R, Ravichandran K S and An K 2000 *Journal of Thermal Spray Technology* **9** 204–9
[10] Anstis G R, Chantikul P, Lawn B R and Marshall D B 1981 *Journal of American Ceramic Society* **64(9)** 533–8

[11] Desiraju G R, Vittal J J and Ramanan A 2011 *Crystal Engineering* World Scientific Publishing Co. Pte. Ltd. Singapore
[12] Gabbott P 2008 *A Practical Introduction to Scanning Differential Calorimetry* Blackwell Publishing Ltd. United Kingdom
[13] Vassen R, Cao X, Tietz F, Basu D and Stöver D 2000 *Journal of American Ceramic Society* **83(8)** 2023–28